Structural, thermodynamics, and mechanistic insights into a tobacco-waste derived activated carbon/polysaccharide composite sponge for efficient Cr(VI) adsorption and reusability

Table S1. Chemical name, formula, and company.

Chemical name	Formula	Company
Carboxymethyl cellulose		Sigma-Aldrich, Germany
Itaconic acid	$C_5H_6O_4$	Sigma-Aldrich, Germany
Guar gum	$(C_6H_{10}O_5)_n$.	Sigma-Aldrich, Germany
Potassium dichromate	$K_2Cr_2O_7$	Sigma-Aldrich, Germany
Methanol	CH_3OH	LOBA CHEMIE PVT.LTD, India
Ethanol	C_2H_6O	Sigma-Aldrich, Germany
Sodium hydroxide (99%, AR)	NaOH	Chimmed, Russia
Hydrochloric acid (37%, AR)	HCl	LOBA CHEMIE PVT.LTD, India

Table S2. Instruments and equibments.

Test name	Abbrevation	Instrument name	Company	Illustration
Fourier transformer infrared	FT-IR	A Nicolet IS10 Fourier transform infrared (FTIR) spectrometer	Thermo Fisher Scientific, Waltham, MA, USA	equipped with an attenuated total reflectance accessory and which ran in the 4000-400 cm^{-1} range was used to gather FTIR spectra
Powered X-ray diffraction	PXRD	Siemens diffractometer (model D500, Germany)	Germany	patterns were captured from powder samples through the use of a Siemens diffractometer (model D500, Germany) that was fitted with a Cu-K radiation source (wavelength 1.54 Angstroms (Å)) operating at 30 kV and 20 mA.
Scanning Electron Microscope	SEM	(JSM-6510LV, JEOL Ltd., Tokyo, Japan)	JEOL Ltd., Tokyo, Japan	The morphology of the investigated sorbents was analyzed with the use of a scanning electron microscope
X-ray photoelectron spectroscopy	XPS	K-ALPHA (Themo Fisher Scientific, USA)	Themo Fisher Scientific, USA	Used for determination the elemental analysis for the compound
Braunnar Emmet Teller	BET	Quantachrome Instruments, Anton Paar Quanta Tec, Inc., Boynton Beach, FL,	Quanta Tec, Inc., Boynton Beach, FL, USA	was utilised for surface and pore analysis (Brunauer Emmett-Teller (BET) surface area, porous volume, and pore size), and NovaWin Software (v11.0) was used for data interpretation.

		USA		The BET surface area of material adsorbents was obtained by the application of nitrogen adsorption-desorption isotherms at 77K through the use of a specific analyser (Quadrasorb–EVO, Quantachrome, USA).
Flame atomic absorption spectrometer		PerkinElmer PinAAcle 500	Singapore	Measuring the concentration of the adsorbate soulution via using Bear Lambert law
Energy Dispersive X-ray	EDX	Leo1430VP microscope	Carl Zeiss AG, Jena, Germany	Elemntal analysis of the material
Transmission electron microscopy	TEM	TEM, FEI Teanci G2 F20, USA	FEI Teanci G2 F20, USA	Determination the morphology of the material and size
pH meter	pH	HANNA (model 211)	USA	Measuring the acidity or basicity of the solution
Sonication	Ultrasonic	Elmasonic P300H ultrasonic bath, continuous mode, power 380 W	Elma Schmidbauer GmbH, Singen, Germany	Sonication of the material as well as used ton disperse material on the solution as it decrease the particle size of the material
Water bath	Shaking	GFL Orbital Shaker 3017		

Table S3. True variables, codes, and their BBD levels.

Code	Variables	-1	0	+1
A	pH	2	5	8
B	Dose (g)	0.02	0.25	0.5
C	Time (min.)	5	55.5	100

Table S4. Equations used in this work to fit the data of adsorption experiments.

Serial	Equation	Nmae	Description	Ref.
1	$q_e = \frac{q_m}{1 + K_L C_e}$	Langmuir	q_e (mg.g^{-1}) Adsorption capacity, C_e equilibrium concentration, q_m (mg.g^{-1}) is the monolayer saturation capacity constant and K_L (L/mg) is the Langmuir constant associated with the free adsorption energy. The favorability of the adsorption process in the Langmuir model is determined by means of the R_L dimensionless factor ($R_L = 1/(1 + k_L \cdot C_0)$) as follows: $R_L = 0$, $0 < R_L < 1$, $R_L = 1$, and $R_L > 1$ indicating irreversible, favorable, linear, and unfavorable adsorption isotherms, respectively.	[1]
2	$q_e = K_F C_e^{\frac{1}{n}}$	Freundlich	K_F Freundlich isotherm constants [(mg/g)/(mg/L)$^{1/n}$], and $1/n$ represents the exponent of non-linearity (i.e., C-type, L-type, and S-type isotherms). n is the Freundlich constants, and $n < 1$ indicates poor adsorption while n = 1–2 and n = 2–10 indicate average and good adsorptions, respectively. The values of n and k_f are calculated, respectively	[2]
3	$q_e = q_m \exp(-\beta\varepsilon^2)$ $\varepsilon = RT ln\left(1 + \frac{1}{C_e}\right)$ $E_{DR} = \sqrt{\frac{1}{2K_{DR}}}$	Dubinin–Radushkevich	q_D is the maximum monolayer adsorption capacity (mg/g), B_D is the activity coefficient related to the apparent free energy of adsorbate adsorption onto the adsorbent (mol^2/kJ^2), ε_D is the Polanyi potential which is related to the equilibrium concentration, and E is the mean adsorption energy.	[3]
4	$q_e = Q_{max} \frac{RT}{b} \ln(K_T C_e)$	Temkin	K_T is the Temkin isotherm constant or equilibrium binding constant (L/mg) corresponding to the maximum binding energy, and b_T is the Temkin isotherm constant related to the heat of adsorbate adsorption onto the adsorbent due to adsorbent-adsorbate interaction (J/mol), R is the gas constant (8.314 J/mol/K), and T is the absolute temperature (herein 298 K).	[4]

5	$q_t = q_m \frac{KC_e}{((1+(KC_e)^n)^{1/n}}$	Jossens	The Jossens isotherm model is a semi-empirical equation used to describe adsorption processes occurring on heterogeneous surfaces, where the energy of adsorption sites is not uniform. Its non-linear form is given by the equation where qe is the amount of adsorbate adsorbed per unit mass of adsorbent at equilibrium (mg/g), Ce is the equilibrium concentration of the adsorbate in solution (mg/L), q_{max} is the theoretical maximum adsorption capacity (mg/g), K is the Jossens isotherm constant related to adsorption affinity (L/mg), and nn is a dimensionless exponent indicative of the surface heterogeneity. A value of n=1 implies a homogeneous adsorption surface and reduces the model to the Langmuir isotherm, while values of n < 1 reflect increasing heterogeneity in adsorption energies. This model effectively captures adsorption behaviors in systems with energetically diverse sites and can describe both monolayer and multilayer adsorption scenarios, making it useful for interpreting complex adsorption processes on irregular surfaces.	
6	$q_e = \frac{q_m k_T c_e}{(1+(K_L C_e)t)1/t}$	Toth	q_e: amount of adsorbate adsorbed at equilibrium (mg/g), Ce:equilibrium concentration of adsorbate in solution (mg/L) q_{max}: theoretical maximum adsorption capacity (mg/g) K_T: Toth isotherm constant related to affinity (L/mg) t t: heterogeneity parameter (dimensionless)	[5]
8	$q_t = q_e\left(1 - e^{K_1 t}\right)$	Pseudo-First-order kinetic	q_e and q_t are the adsorption capacities at equilibrium and time t (mg/g), and k_1 is the rate constant (min^{-1}), respectively.	[6]
9	$q_t = \frac{tK_2 q_e^2}{1+q_e K_2 t}$	Pseudo-Second-order kinetic	k_2 is the pseudo-second order constant (mg/(g.min))	[7]
10	$q_t = K_i t^{1/2} + X$	Intraparticle diffusion	q_t is the adsorption capacity at time t in (mg/g), k_{int} is the intraparticle diffusion rate constant ($mg \cdot g^{-1} \cdot min^{-1/2}$), and C is a constant related to the the thickness of the boundary layer (mg/g).	[8]
10	$q_t = \frac{1}{\beta}\ln(\alpha\beta t + 1)$	Elovich	The constants α chemical adsorption rate ($mg.g^{-1}min^{-1}$), and β Coefficient in relation with extension of covered surface	[9]
12	$\Delta G^o = \Delta H^o - T\Delta S^o$	Gibbs free energy	ΔG°: Gibbs free energy change; K_d: equilibrium constant; R: gas constant;	[10]

			T: temperature.	
13	$LnK_d = \frac{\Delta S^{\circ}}{R} - \frac{\Delta H^{\circ}}{RT}$	Van't Hoff	ΔS°: entropy change; ΔH°: enthalpy change.	[11]
14	$LnK_d = lnA - (\frac{Ea^0}{R})\frac{1}{T}$	Arhinus	E_a was the activation energy, A Arhinus constant, R ideal gas constant 8.314 J/mol.K, T (K) is the absolute solution temperature	[12]

Table S5. List of abbreviation.

Symbol	Definition
q_e	the adsorbed amount of dye at equilibrium concentration ($mg.g^{-1}$)
q_{mL}	the maximum sorption capacity (corresponding to the saturation of the monolayer, ($mg.g^{-1}$)
K_L	Langmuir binding constant which is related to the energy of sorption (L/mg)
C_e	is the equilibrium concentration of dyes in solution
K_F	Freundlich constants related to the sorption capacity (mg/g) $(L/mg)^{1/n}$
n	intensity
K_{DR}	constant related to the sorption energy ($mol^2k\ J\text{-}^2$)
q_{DR}	theoretical saturation capacity (mg/g)
ε	Polanyi potential (J^2mol^{-2})
R	Gas constant (8.314 $J.mol^{-1}K^{-1}$)
T	temperature where the adsorption occurs
A_T	Temkin isotherm constant
b_T	Temkin constant in relation to heat of adsorption ($J.mol^{-1}$)
q_t	is the amount of dye adsorbed ($mmol.g^{-1}$)
K_1	Rate constant for Pseudo first order constant for the adsorption processes (min^{-1})
q_2	Maximum adsorption capacity for pseudo second order
K_2	Rate constant for Pseudo first order constant for the adsorption processes ($g.mg^{-1}min^{-1}$)
α	Chemical adsorption rate ($mg.g^{-1}min^{-1}$)
β	Coefficient in relation with extension of covered surface
ΔG^o	Free Gibb's energy
ΔH^o	Enthalpy
ΔS^o	Entropy
K_c	distribution coefficient
C_{eq}	Concentration at equilibrium (mg/L)

Table S6. The parameter of the adsorption isotherm for Cr(VI) onto TAC and TACGC composite sponge.

Isotherm	Value of parameters	TACGC	TAC
Langmuir	$q_{m\ exp}$ (mg/g)	402.97	319.8
	q_m (mg/g)	404.87	322.7
	K_L (L/mg)	0.05896	0.029
	R_L	0.077	0.62
	Reduced Chi-Sqr	176.41808	408.32334
	Residual Sum of Squares	2822.68925	6533.17342
	R-Square (COD)	0.99075	0.96716
	R^2	0.99017	0.9651
Freundlich	n	3.32	2.8
	K_F (mg/g) $(L/mg)^{1/n}$	91.65	53.19
	Reduced Chi-Sqr	934.7486	1430.87717
	Residual Sum of Squares	14955.97755	22894.0348
	R-Square (COD)	0.95099	0.88491
	R^2	0.94793	0.87772
Dubinin–Radushkevich	$Q_{DR}(mg.g^{-1})$	377.84	312.6
	K_{DR} ($mol^2k\ J^{-2}$)	2.076E-5	5.52E-5
	Ea (kJ/mol)	33.6	31.4
	Reduced Chi-Sqr	1223.10442	347.35089
	Residual Sum of Squares	19569.67072	5557.61426
	R-Square (COD)	0.93588	0.97206
	R^2	0.93187	0.97032
Temkin	b_T (J/mol)	33.22	27.58
	K_T (L/mol)	1.46	0.244
	Reduced Chi-Sqr	691.64264	602.84619
	Residual Sum of Squares	11066.28218	9645.5391
	R-Square (COD)	0.96374	0.95151
	R^2	0.96147	0.94848
Jossens	K (L/mg)	24.49	7.91

	n	0.047	0.026
	Reduced Chi-Sqr	184.30081	142.56845
	Residual Sum of Squares	2764.51209	2138.52671
	R-Square (COD)	0.99094	0.98925
	R^2	0.98973	0.98782
Toth	q_m	438.94	322.16
	K_T (L/mg)	21.54	15.85
	t	1.06	2.84
	Reduced Chi-Sqr	186.73013	70.56349
	Residual Sum of Squares	2800.95196	1058.45235
	R-Square (COD)	0.99082	0.99468
	R^2	0.9896	0.99397

Table S7. Models of adsorption kinetic parameters of Cr(VI) onto TAC and TACGC composite sponge.

Model	Value of parameters	TACGC	TAC
Pseudo-First-order kinetic	K_1 (min^{-1})x10^{-2}	0.0495	343.39
	Reduced Chi-Sqr	48.26717	113.52575
	Residual Sum of Squares	917.07619	2156.98921
	R-Square (COD)	0.99644	0.98966
	R^2	0.99625	0.98911
Pseudo-second-order kinetic	K_2 ($g.mg^{-1}min^{-1}$)x10^{-2}	9.68136E-5	5.68E-5
	q_e (mg/g)	404.85	323.2
	Reduced Chi-Sqr	959.59977	213.81296
	Residual Sum of Squares	18232.39565	4062.44633
	R-Square (COD)	0.94257	0.98052
	R^2	0.93955	0.9795
Intraparticle diffusion	K_i ($mg.g^{-1}min^{1/2}$)	40.38	35.44
	X (mg/g)	57.78	36.82

	Reduced Chi-Sqr	1146.06071	647.45005
	Residual Sum of Squares	21775.15348	12949.00091
	R-Square (COD)	0.91545	0.93792
	R^2	0.911	0.93792
Elovich	β (g/mg)	108.58	109.57
	α ($mg.g^{-1}min^{-1}$)	0.0048	0.002
	Reduced Chi-Sqr	182.68785	163.64278
	Residual Sum of Squares	3471.0691	3109.21287
	R-Square (COD)	0.98652	0.98509
	R^2	0.98581	0.98431
Experimental data	q_e (exp) (mg/g)	406.22	326.6

Table S8. The thermodynamic parameters.

T (K)	ΔG° (kJ/mol)	ΔH° (kJ/mol)	ΔS° (J/mol.K)
293	-1.94814		
298	-3.57602	93.45	325.57
303	-5.2039		
308	-6.83178		
313	-8.45966		
318	-10.0875		

Table S9. Analyzing similar adsorbents for the absorption of Cr(VI).

Adsorbent Material	Biomass Source	Preparation / Modification	Optimal pH	Maximum Adsorption Capacity (mg/g)	Reference
Activated carbon from orange peel	Citrus waste	H_3PO_4 activation	2.0	97.32	[1]
Banana peel biochar	Fruit waste	Pyrolysis at 450 °C	2.0	58.8	[2]
Rice husk activated carbon	Agro-waste	KOH activation	2.0	123.5	[3]

Sawdust biochar	Wood waste	Pyrolysis	2–3	43.0	[4]
Coconut shell AC	Agricultural waste	Steam activation	2	74.6	[5]
Chitosan–alginate composite	Marine waste	Hydrogel crosslinking	3–4	263.2	[6]
Tea waste activated carbon	Beverage waste	Carbonization	2	42.1	[7]
Sugarcane bagasse biochar	Agro-residue	Pyrolysis	2	35.0	[8]
Pine cone activated carbon	Forest residue	H_3PO_4 activation	2	92.5	[9]
Neem leaf powder	Plant biomass	Drying & milling	2	15.87	[10]
Spirulina biomass	Microalgae	Drying & activation	2	81.3	[11]
TAC	Tobacco waste	KOH activation	4	322.7	**This study**
TACGC composite sponge (**This study**)	Tobacco + GG–CMC–IA	Polymer crosslinking	4	404.87	**This study**

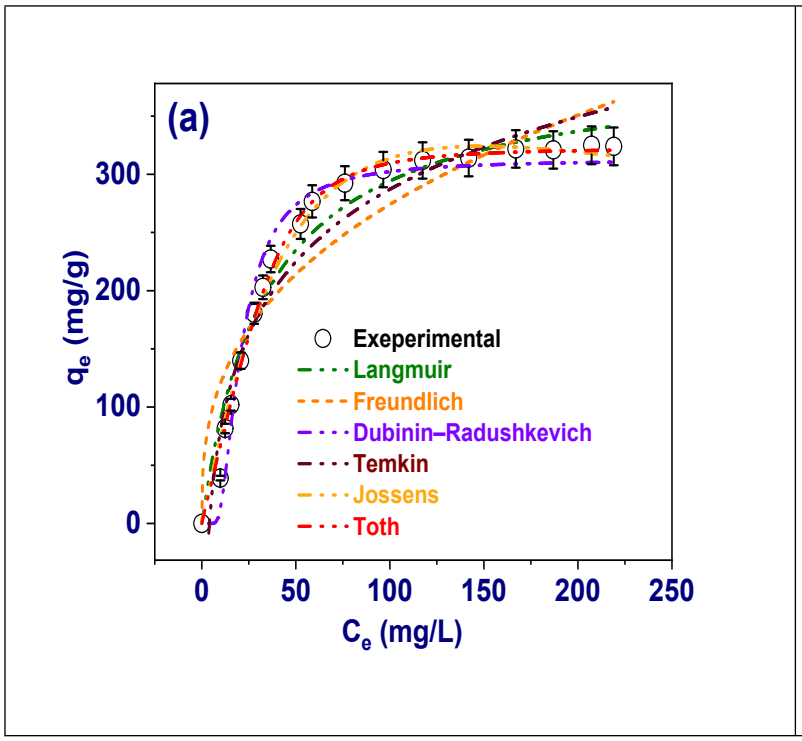

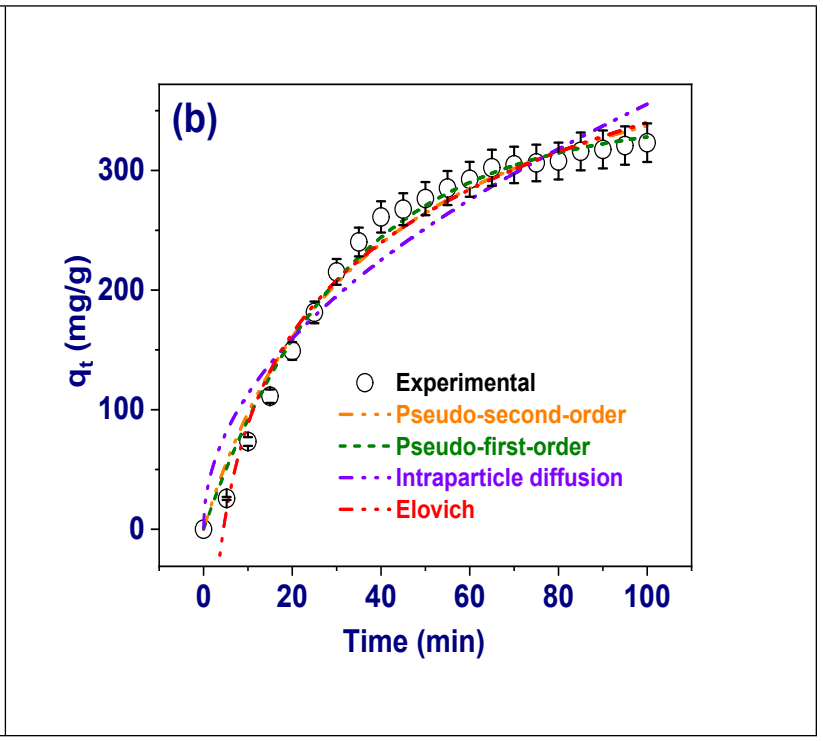

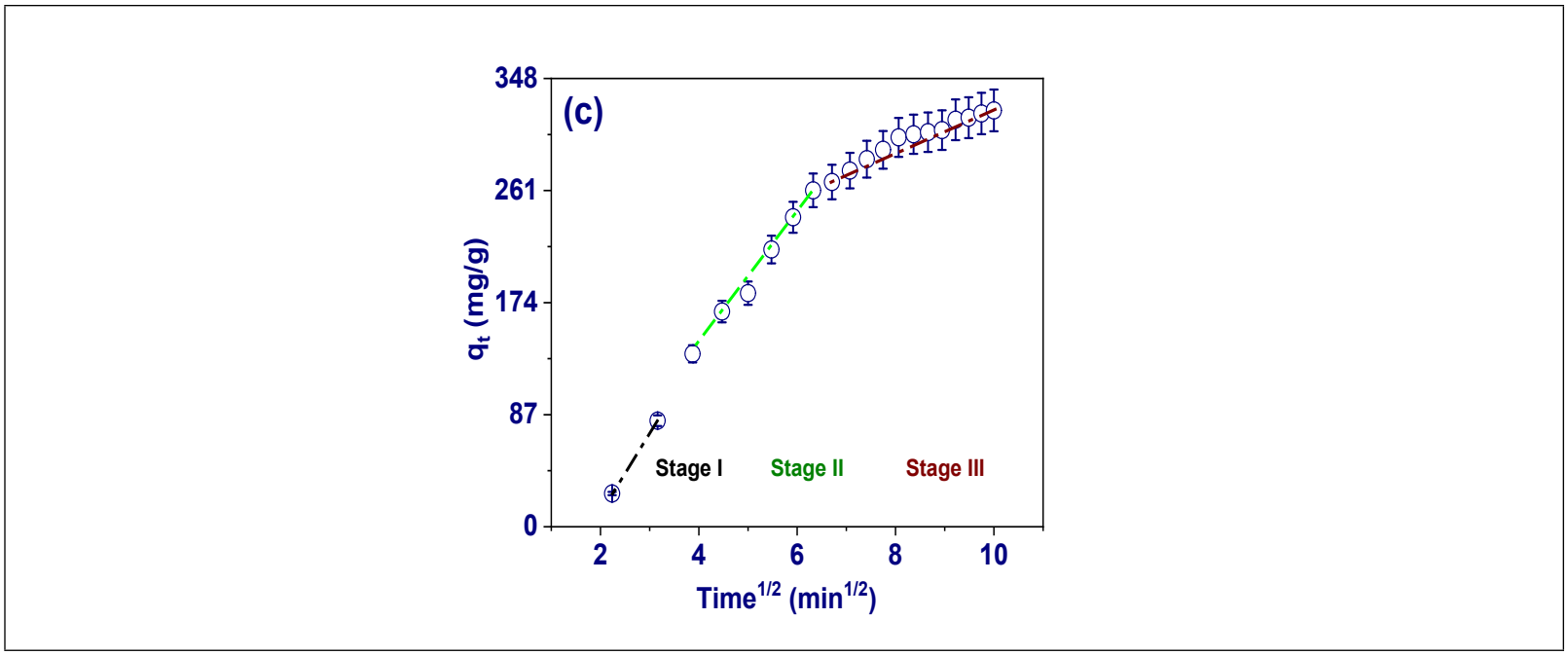

Fig. S1. (a) Adsorption isotherms models, (b) Adsorption kinetics models, and (c) Intraparticle diffusion on adsorption of Cr(VI) onto TAC.

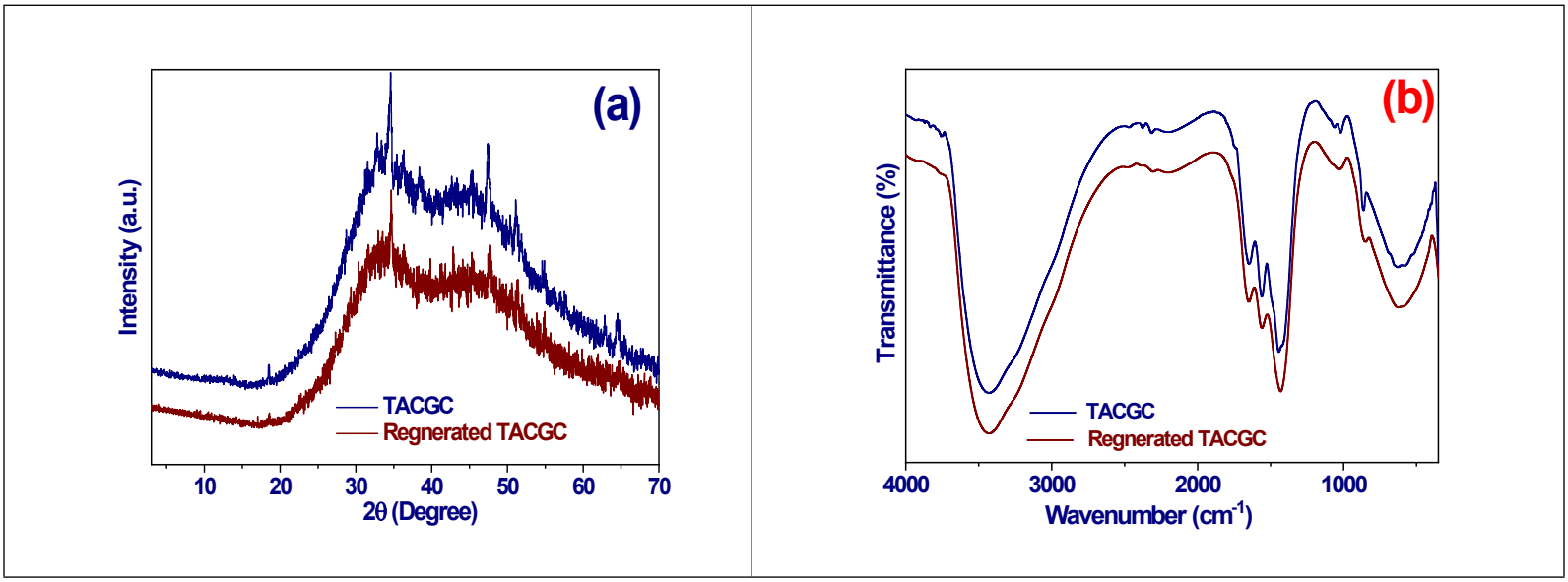

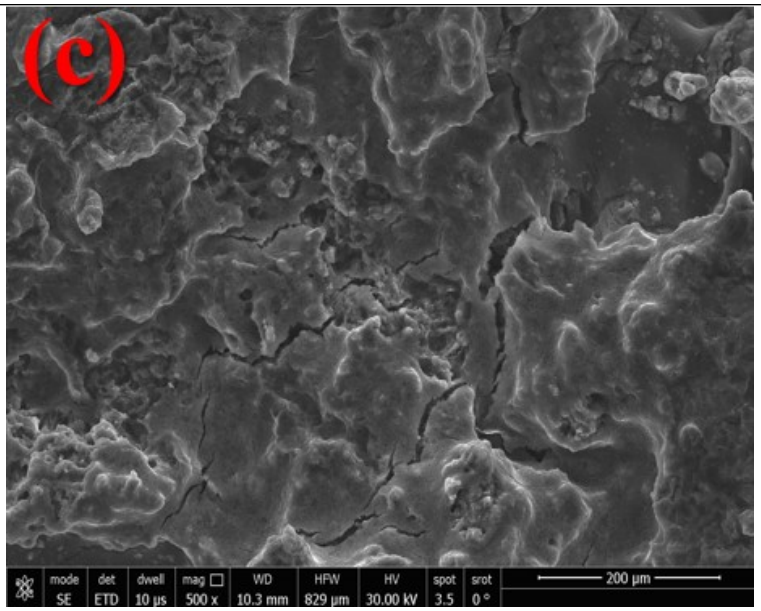

Fig. S2. (a) XRD, (b) FT-IR of TACGC and regenerated TACGC, and (c) SEM of regenerated TACGC.

References

[1] I. Langmuir, The constitution and fundamental properties of solids and liquids. Part I. Solids, J. Am. Chem. Soc., 38 (1916) 2221-2295.
[2] H.M.F. Freundlich, Over the adsorption in solution, J. Phys. Chem., 57 (1906) 385-471.
[3] M. Dubinin, The equation of the characteristic curve of activated charcoal, Proc. Acad. Sci. USSR Phys. Chem. Sect., 55 (1947) 327-329.
[4] V.P. M.I. Tempkin, Kinetics of ammonia synthesis on promoted iron catalyst, Acta Phys. Chim. USSR, 12 (1940) 327-356.
[5] D.P. Vargas, L. Giraldo, J.C. Moreno-Piraján, CO_2 adsorption on activated carbon honeycomb-monoliths: a comparison of Langmuir and Toth models, International journal of Molecular Sciences, 13 (2012) 8388-8397.
[6] S.K. Lagergren, About the theory of so-called adsorption of soluble substances, Sven. Vetenskapsakad. Handingarl, 24 (1898) 1-39.
[7] Y.-S. Ho, G. McKay, Sorption of dye from aqueous solution by peat, Chemical Engineering Journal, 70 (1998) 115-124.
[8] W.J. Weber Jr, J.C. Morris, Kinetics of adsorption on carbon from solution, J. Sanit. Eng. Div., 89 (1963) 31-59.
[9] M.H. Dehghani, A. Dehghan, A. Najafpoor, Removing Reactive Red 120 and 196 using chitosan/zeolite composite from aqueous solutions: Kinetics, isotherms, and process optimization, Journal of Industrial and Engineering Chemistry, 51 (2017) 185-195.
[10] E.C. Lima, A. Hosseini-Bandegharaei, J.C. Moreno-Piraján, I. Anastopoulos, A critical review of the estimation of the thermodynamic parameters on adsorption equilibria. Wrong use of equilibrium constant in the Van't Hoof equation for calculation of thermodynamic parameters of adsorption, Journal of Molecular Liquids, 273 (2019) 425-434.

[11] H.N. Tran, S.-J. You, A. Hosseini-Bandegharaei, H.-P. Chao, Mistakes and inconsistencies regarding adsorption of contaminants from aqueous solutions: a critical review, Water Research, 120 (2017) 88-116.
[12] B. Oladipo, E. Govender-Opitz, T.V. Ojumu, Kinetics, thermodynamics, and mechanism of Cu (II) ion sorption by biogenic iron precipitate: using the lens of wastewater treatment to diagnose a typical biohydrometallurgical problem, ACS Omega, 6 (2021) 27984-27993.
[13] Y. Zheng, B. Cheng, W. You, J. Yu, W. Ho, 3D hierarchical graphene oxide-NiFe LDH composite with enhanced adsorption affinity to Congo red, methyl orange and Cr (VI) ions, Journal of Hazardous Materials, 369 (2019) 214-225.
[14] Y. Lu, B. Jiang, L. Fang, F. Ling, J. Gao, F. Wu, X. Zhang, High performance NiFe layered double hydroxide for methyl orange dye and Cr (VI) adsorption, Chemosphere, 152 (2016) 415-422.
[15] M. Liu, T. Wen, X. Wu, C. Chen, J. Hu, J. Li, X. Wang, Synthesis of porous Fe 3 O 4 hollow microspheres/graphene oxide composite for Cr (VI) removal, Dalton Transactions, 42 (2013) 14710-14717.
[16] M. Su, Y. Fang, B. Li, W. Yin, J. Gu, H. Liang, P. Li, J. Wu, Enhanced hexavalent chromium removal by activated carbon modified with micro-sized goethite using a facile impregnation method, Science of the Total Environment, 647 (2019) 47-56.
[17] L. Zhang, F. Fu, B. Tang, Adsorption and redox conversion behaviors of Cr(VI) on goethite/carbon microspheres and akaganeite/carbon microspheres composites, Chemical Engineering Journal, 356 (2019) 151-160.
[18] J. Zhao, Y. Tan, K. Su, J. Zhao, C. Yang, L. Sang, H. Lu, J. Chen, A facile homogeneous precipitation synthesis of NiO nanosheets and their applications in water treatment, Applied Surface Science, 337 (2015) 111-117.
[19] P. Karthikeyan, K. Ramkumar, K. Pandi, A. Fayyaz, S. Meenakshi, C.M. Park, Effective removal of Cr (VI) and methyl orange from the aqueous environment using two-dimensional (2D) Ti3C2Tx MXene nanosheets, Ceramics International, 47 (2021) 3692-3698.
[20] Z. Wu, C. Zhao, W. Zeng, X. Wang, C. Liu, Z. Yu, J. Zhang, Z. Qiu, Ultra-high selective removal of CR and Cr (VI) from aqueous solutions using polyethyleneimine functionalized magnetic hydrochar: Application strategy and mechanisms insight, Chemical Engineering Journal, 448 (2022) 137464.
[21] S. Adil, J.-O. Kim, Enhanced adsorption performance of a Cu/Ni-MXene composite for phosphate recovery and removal of Cr(VI) from aqueous solutions, Separation Purification Technology, 326 (2023) 124725.
[22] A.M. Alsuhaibani, A.A. Alayyafi, L.A. Albedair, M.G. El-Desouky, A.A. El-Bindary, Efficient fabrication of a composite sponge for Cr(VI) removal via citric acid cross-linking of metal-organic framework and chitosan: adsorption isotherm, kinetic studies, and optimization using Box-Behnken design, Materials Today Sustainability, 26 (2024) 100732.